INTERNATIONAL JOURNAL FOR NUMERICAL METHODS IN FLUIDS, VOL. 17, 271–289 (1993)

A LEAST-SQUARES FINITE ELEMENT METHOD FOR TIME-DEPENDENT INCOMPRESSIBLE FLOWS WITH THERMAL CONVECTION

LI Q. TANG AND TATE T. H. TSANG

Department of Chemical Engineering, University of Kentucky, Lexington, KY 40506-0046, U.S.A.

SUMMARY

The time-dependent Navier–Stokes equations and the energy balance equation for an incompressible, constant property fluid in the Boussinesq approximation are solved by a least-squares finite element method based on a velocity–pressure–vorticity–temperature–heat-flux ($\mathbf{u}$–P–ω–T–$\mathbf{q}$) formulation discretized by backward finite differencing in time. The discretization scheme leads to the minimization of the residual in the l^2-norm for each time step. Isoparametric bilinear quadrilateral elements and reduced integration are employed. Three examples, thermally driven cavity flow at Rayleigh numbers up to 10^6, lid-driven cavity flow at Reynolds numbers up to 10^4 and flow over a square obstacle at Reynolds number 200, are presented to validate the method.

KEY WORDS Least-squares finite element method Time-dependent Incompressible flows Boussinesq approximation Navier–Stokes equations

1. INTRODUCTION

The past decade has witnessed a great deal of progress in the area of computational fluid dynamics. Numerous flow problems have been successfully solved by finite difference, finite volume and finite element methods. Most finite element methods are based on the Galerkin method,[1,2] the Taylor–Galerkin method and the Petrov–Galerkin method.[3–5] Mixed-order interpolation and penalty approach are commonly used in these methods. It is well known that these methods often lead to large, sparse, unsymmetric linear systems which are difficult to solve numerically. This explains why finite element analysis for three-dimensional fluid flow problems is not a common practice. To overcome this difficulty, we propose and develop a Least-Squares Finite Element Method (LSFEM) for time-dependent incompressible flow problems. The linear systems resulting from the discretization of LSFEM are always symmetrical and positive-definite. Therefore, they can be solved more easily and efficiently. This is the main reason for investigating the least-squares finite element approach.

Least-squares finite element methods have already been applied with some success to compressible Euler and hyperbolic equations. Jiang and Carey[6,7] and Jiang and Povinelli[8] used an implicit method for compressible flows. To further the capabilities of the method, Lefebvre *et al.*[9] applied unstructured triangular meshes to compressible flow problems. For transient advection problems, Donea and Quartapelle[10] classified four different LSFEM approaches: characteristic LSFEM proposed by Li,[11] LSFEM by Carey and Jiang,[12] Taylor LSFEM by Park and Liggett[13] and space–time LSFEM by Nguyen and Reynen.[14]

0271–2091/93/160271–19$14.50

Received 23 June 1992
Revised 1 March 1993

For steady-state incompressible flows, an error analysis of LSFEM formulation for the Stokes problem was presented by Chang and Jiang[15] and Jiang and Chang.[16] Jiang[17] used LSFEM for lid-driven cavity flow at Reynolds numbers up to 10 000, and for flow over a backward facing step at Reynolds numbers up to 900. He validated his results of lid-driven cavity flow with Ghia *et al.*,[18] Gresho *et al.*,[19] Kim[20] and Sohn *et al.*[21] He also tested two outflow boundary conditions for flow over the backward facing step. Good results were obtained. Lefebvre *et al.*[9] used 40×40 quadratic triangular elements together with an incomplete Cholesky conjugate gradient algorithm for the lid-driven cavity problem.

In this work, our objectives are twofold. First, we extend the LSFEM by Carey and Jiang[12] and Jiang[17] to time-dependent incompressible flow problems. Previous LSFEM results by Jiang[17] and Jiang and Povinelli[8] were obtained from a steady-state LSFEM algorithm. For high Reynolds number flows, time-dependent algorithms can provide interesting dynamic flow behaviour. In addition, they do not require a 'good initial guess' or 'zero-order' continuation procedure as many steady-state algorithms do for achieving convergence. Second, we apply the time-dependent LSFEM algorithm to a natural convection problem. The content of the paper is organized as follows. In Section 2, we give a brief account of the time-dependent first-order velocity–pressure–vorticity–temperature–heat-flux formulation. In Section 3, we propose a scheme to discretize the system by minimizing the residual in the l^2-norm. In Section 4, the performance of the time-dependent LSFEM is illustrated by three typical examples: thermally driven cavity flow, lid-driven cavity flow and flow over a square obstacle. The conclusions are finally given in Section 5.

2. FORMULATION

2.1. Governing equations

Let Ω be a bounded domain. The spatial and temporal co-ordinates are denoted by $\mathbf{x}=(x, y, z)\in\bar{\Omega}$ and $t\in[0, \tau]$. We consider the time-dependent incompressible flow with thermal convection using the Boussinesq approximation. The governing equations in dimensionless form are as follows:

$$\nabla\cdot\mathbf{u}=0 \qquad \text{in } \Omega,\ t\geq 0, \tag{1}$$

$$\frac{\partial\mathbf{u}}{\partial t}+\mathbf{u}\cdot\nabla\mathbf{u}+\nabla p-\frac{1}{Re}\nabla^2\mathbf{u}-\frac{1}{Fr}\mathbf{k}T=\mathbf{0} \qquad \text{in } \Omega,\ t>0, \tag{2}$$

$$\frac{\partial T}{\partial t}+\mathbf{u}\cdot\nabla T-\frac{1}{Pe}\nabla^2 T=0 \qquad \text{in } \Omega,\ t>0, \tag{3}$$

where the velocity $\mathbf{u}=(u, v, w)^{\mathrm{T}}$, p is the pressure deviation from hydrostatic at the reference temperature, T the temperature and $\mathbf{k}$ the unit vector in the y direction. The domain $\bar{\Omega}=\Omega\cup\partial\Omega$ and the boundary of the domain $\partial\Omega=\Gamma_1\cup\Gamma_2$. The dimensionless numbers for the thermal convection problems are defined as

$$Fr=\frac{U^2}{\gamma\Delta T g D},$$

$$Pr=\frac{\nu}{\kappa},$$

$$Ra=\frac{\gamma g D^3 \Delta T}{\kappa \nu},$$

$$Re=\sqrt{\frac{Ra}{Pr}},$$

$$Pe=\sqrt{(Ra \cdot Pr)},$$

where Fr is the Froude number, Pr the Prandtl number and Ra the Rayleigh number; U is the characteristic velocity and D the characteristic length of the domain Ω, $\nu=\mu/\rho$ is the kinematic viscosity, κ the thermal diffusivity, γ the volumetric thermal expansion coefficient, ΔT the characteristic temperature difference and g the gravitational acceleration.

2.2. *First-order system*

Introducing the vorticity $\omega=\nabla \times \mathbf{u}$ and heat flux $\mathbf{q}=(q_x, q_y, q_z)^{\mathrm{T}}$, Equations (1)–(3) can be reduced to the following first-order system in order to use simple C^0-elements:

$$\frac{\partial \mathbf{u}}{\partial t}+\mathbf{u}\cdot\nabla\mathbf{u}+\nabla p+\frac{1}{Re}\nabla\times\omega-\frac{1}{Fr}\mathbf{k}T=\mathbf{0}, \tag{4}$$

$$\nabla\cdot\mathbf{u}=0, \tag{5}$$

$$\omega-\nabla\times\mathbf{u}=\mathbf{0}, \tag{6}$$

$$\frac{\partial T}{\partial t}+\mathbf{u}\cdot\nabla T+\nabla\cdot\mathbf{q}=0, \tag{7}$$

$$\mathbf{q}+\frac{1}{Pe}\nabla T=\mathbf{0}. \tag{8}$$

Since the derivatives for velocity, pressure, vorticity, temperature and heat flux are of the same order, we employ the equal-order interpolation function.

We shall only consider the problem on $\Omega \subset \Re^2$ here:

$$\frac{\partial u}{\partial t}+u\frac{\partial u}{\partial x}+v\frac{\partial u}{\partial y}+\frac{\partial p}{\partial x}+\frac{1}{Re}\frac{\partial \omega}{\partial y}=0, \tag{9}$$

$$\frac{\partial v}{\partial t}+u\frac{\partial v}{\partial x}+v\frac{\partial v}{\partial y}+\frac{\partial p}{\partial y}-\frac{1}{Re}\frac{\partial \omega}{\partial x}-\frac{1}{Fr}T=0, \tag{10}$$

$$\frac{\partial u}{\partial x}+\frac{\partial v}{\partial y}=0, \tag{11}$$

$$\omega+\frac{\partial u}{\partial y}-\frac{\partial v}{\partial x}=0, \tag{12}$$

$$\frac{\partial T}{\partial t}+u\frac{\partial T}{\partial x}+v\frac{\partial T}{\partial y}+\frac{\partial q_x}{\partial x}+\frac{\partial q_y}{\partial y}=0, \tag{13}$$

$$q_x+\frac{1}{Pe}\frac{\partial T}{\partial x}=0, \tag{14}$$

$$q_y+\frac{1}{Pe}\frac{\partial T}{\partial y}=0. \tag{15}$$

Equations (9)–(15) form a non-linear initial boundary value problem and can be expressed as

$$A_0\frac{\partial \mathbf{v}}{\partial t}+A_1(\mathbf{v})\frac{\partial \mathbf{v}}{\partial x}+A_2(\mathbf{v})\frac{\partial \mathbf{v}}{\partial y}+A_3\mathbf{v}=\mathbf{0} \qquad \text{in } \Omega,\ t>0, \tag{16}$$

$$B\cdot\mathbf{v}=\mathbf{g} \qquad \text{on } \partial\Omega,\ t\geq 0, \tag{17}$$

$$\mathbf{v}=\mathbf{v}_0 \qquad \text{in } \Omega,\ t=0, \tag{18}$$

where $\mathbf{v}=(u, v, p, \omega, T, q_x, q_y)^{\mathrm{T}}$, $\mathbf{g}$ and $\mathbf{v}_0$ are the given values and the coefficient matrices are given by

$$A_0=\begin{pmatrix} 1&0&0&0&0&0&0\\ 0&1&0&0&0&0&0\\ 0&0&0&0&0&0&0\\ 0&0&0&0&0&0&0\\ 0&0&0&0&1&0&0\\ 0&0&0&0&0&0&0\\ 0&0&0&0&0&0&0 \end{pmatrix}, \qquad A_1=\begin{pmatrix} u&0&1&0&0&0&0\\ 0&u&0&-1/Re&0&0&0\\ 1&0&0&0&0&0&0\\ 0&-1&0&0&0&0&0\\ 0&0&0&0&u&1&0\\ 0&0&0&0&1/Pe&0&0\\ 0&0&0&0&0&0&0 \end{pmatrix}, \tag{19}$$

$$A_2=\begin{pmatrix} v&0&0&1/Re&0&0&0\\ 0&v&1&0&0&0&0\\ 0&1&0&0&0&0&0\\ 1&0&0&0&0&0&0\\ 0&0&0&0&v&0&1\\ 0&0&0&0&0&0&0\\ 0&0&0&0&1/Pe&0&0 \end{pmatrix}, \qquad A_3=\begin{pmatrix} 0&0&0&0&0&0&0\\ 0&0&0&0&-1/Fr&0&0\\ 0&0&0&0&0&0&0\\ 0&0&0&1&0&0&0\\ 0&0&0&0&0&0&0\\ 0&0&0&0&0&1&0\\ 0&0&0&0&0&0&1 \end{pmatrix}. \tag{20}$$

There are two constraints for the incompressible flow:

Constraint 1. The initial velocity value (u_0, v_0) is subject to

$$\left(\frac{\partial}{\partial x}, \frac{\partial}{\partial y}\right)\begin{pmatrix} u_0\\ v_0\end{pmatrix}=0 \qquad \text{in } \Omega. \tag{21}$$

Constraint 2. The initial value $\mathbf{v}_0$ and the boundary value $\mathbf{g}$ are subject to, along the boundary,

$$\mathbf{n}\cdot(B\cdot\mathbf{v}_0)=\mathbf{n}\cdot\mathbf{g} \qquad \text{in } \partial\Omega. \tag{22}$$

If either equation (21) or (22) is violated, the Navier–Stokes problem is ill-posed and has no solution.[22]

In the formulation of other finite element weak solutions, integration by parts generates additional boundary terms, whereas LSFEM does not use integration by parts in the formulation. Therefore, no additional boundary integration term results. Since the system is of first order, only Dirichlet-type boundary conditions are specified in LSFEM. If stress boundary conditions are specified, we can use shear stresses instead of vorticity to formulate the first-order system of equations, thus leading to Dirichlet-type boundary conditions. In the context of LSFEM, Jiang[17] had discussed different boundary conditions for a variety of fluid flows.

The discretization of equation (16) by backward finite difference in time leads to the implicit problem with the first-order accuracy $O(\Delta t)$,

$$A_0\frac{(\mathbf{v}^{n+1}-\mathbf{v}^n)}{\Delta t}+A_1^n\frac{\partial \mathbf{v}^{n+1}}{\partial x}+A_2^n\frac{\partial \mathbf{v}^{n+1}}{\partial y}+A_3\mathbf{v}^{n+1}=\mathbf{0} \tag{23}$$

or

$$L\mathbf{v}^{n+1}=\mathbf{f}^n, \tag{24}$$

where time step $\Delta t=t^{n+1}-t^n$, and n denotes the nth time level. L is a first-order partial differential operator, defined by

$$L=A_1^n\frac{\partial}{\partial x}+A_2^n\frac{\partial}{\partial y}+\left(\frac{A_0}{\Delta t}+A_3\right) \tag{25}$$

and the right-hand-side vector

$$\mathbf{f}^n=\frac{A_0}{\Delta t}\mathbf{v}^n.$$

It should be noted that equation (23) is linearized by setting $A_1^n=A_1(\mathbf{v}^n)$ and $A_2^n=A_2(\mathbf{v}^n)$ at the previous time level.

3. LEAST-SQUARES DISCRETIZATION

To develop time-dependent LSFEM systems, we define the least-squares functional of the residual $\mathbf{R}=L\mathbf{v}^{n+1}-\mathbf{f}^n$ in equation (23) for admissible $\mathbf{v}^{n+1}$ as

$$J(\mathbf{v}^{n+1})=\int_\Omega \mathbf{R}^{\mathrm{T}}\cdot\mathbf{R}\,\mathrm{d}x\,\mathrm{d}y. \tag{26}$$

Minimization of the functional leads to

$$\delta J(\mathbf{v}^{n+1})=0,$$

i.e.

$$\int_\Omega [L(\delta\mathbf{v}^{n+1})]^{\mathrm{T}}\cdot[L\mathbf{v}^{n+1}-\mathbf{f}^n]\,\mathrm{d}x\,\mathrm{d}y=0. \tag{27}$$

Setting $\delta\mathbf{v}^{n+1}=\mathbf{w}$, equation (27) can be rewritten as

$$(L\mathbf{w},\, L\mathbf{v}^{n+1})=(L\mathbf{w},\, \mathbf{f}^n). \tag{28}$$

Let us discretize the domain Ω by a union of finite elements Ω^e as $\Omega=\bigcup_{e=1}^{N_e}\Omega^e$ and introduce the equal-order interpolation function $\Phi_i(x, y)$. The approximation solution is defined as

$$\mathbf{v}_h^{n+1}(x, y, t)=\sum_{i=1}^{N_n}\Phi_i(x, y)\begin{bmatrix} u_i(t)\\ v_i(t)\\ p_i(t)\\ \omega_i(t)\\ T_i(t)\\ q_{xi}(t)\\ q_{yi}(t)\end{bmatrix} \tag{29}$$

and the test function is chosen as

$$\mathbf{w}(x, y, t)=\Phi_i(x, y)\{1\}, \tag{30}$$

where N_n is the number of nodes for an element. Substituting equations (29) and (30) into (28), we have the quasi-linear algebraic equations

$$K^n \cdot U^{n+1} = F^n, \tag{31}$$

where

$$K^n = (L\Phi_i, L\Phi_j) = \sum_{e=1}^{N_e} \int_{\Omega^e} (L\Phi_i)^{\mathrm{T}} (L\Phi_j)\, \mathrm{d}x\, \mathrm{d}y. \tag{32}$$

The global matrix K^n, vector U^{n+1} and right-hand-side vector F^n are assembled by the following element matrices and vectors:

$$(K_{ij}^n)^e = \int_{\Omega^e} (L\Phi_i)^{\mathrm{T}} (L\Phi_j)\, \mathrm{d}x\, \mathrm{d}y, \tag{33}$$

$$(U_j^{n+1})^e = \begin{bmatrix} u_j^{n+1} \\ v_j^{n+1} \\ p_j^{n+1} \\ \omega_j^{n+1} \\ T_j^{n+1} \\ q_{xj}^{n+1} \\ q_{yj}^{n+1} \end{bmatrix}^e, \tag{34}$$

$$(F_i^n)^e = \int_{\Omega^e} (L\Phi_i)^{\mathrm{T}} \cdot \frac{1}{\Delta t} \begin{bmatrix} u^n \\ v^n \\ 0 \\ 0 \\ T^n \\ 0 \\ 0 \end{bmatrix}^e \mathrm{d}x\, \mathrm{d}y \tag{35}$$

and

$$L\Phi_i = A_1^n \frac{\partial \Phi_i}{\partial x} + A_2^n \frac{\partial \Phi_i}{\partial y} + \left(\frac{A_0}{\Delta t} + A_3 \right) \Phi_i, \tag{36}$$

where u^n, v^n and T^n are calculated at the nth time level.

An important feature of the LSFEM can be observed from equation (33) that coefficient matrix K^n is symmetric and positive-definite. Therefore, only the lower half band of the matrix is generated by reduced integration[23] and stored for the Cholesky factorization. Like Jiang's results for the steady-state incompressible flows,[17] our unsteady-state solutions also reveal that pressure, vorticity and heat flux have some oscillations at nodal points but the solutions at Gaussian points are very smooth. We test two smoothing techniques: one is a simple average method at Gaussian point (x_G, y_G),

$$\begin{bmatrix} p_G \\ \omega_G \\ q_{x_G} \\ q_{y_G} \end{bmatrix} = \frac{1}{N_n} \sum_{i=1}^{N_n} \begin{bmatrix} p_i \\ \omega_i \\ q_{xi} \\ q_{yi} \end{bmatrix},$$

and the other is called element area weighting, described by Sani *et al.*[24] Both smoothing techniques work very well. But for LSFEM, the above smoothing technique is simple to use.

4. RESULTS AND DISCUSSIONS

In testing our time-dependent LSFEM algorithm with these 'classic' examples, we use the following criterion to obtain steady-state solutions:

$$\max_{1 \le i \le N_v} |u_i^{n+1} - u_i^n| < \varepsilon, \tag{37}$$

where i denotes the ith node and N_v is the total number of unknowns. The tolerance ε is chosen as 10^{-6} for the thermally driven cavity flow and as 10^{-4} for the lid-driven cavity flow and the flow over a square obstacle. It is assumed that the numerical solutions approach the steady state when the criterion is satisfied. The method used to solve the time-dependent matrix system is similar to that for solving steady-state problems by the successive substitution without under-relaxation. Since the backward differencing method is unconditionally stable, a large time step $\Delta t \ge 0{\cdot}5$ can be applied in all examples. The dependent variables do not have significant changes as the flow approaches steady-state condition; therefore, we can use large Δt in the latter part of the simulations. In addition to equation (37), we have also used another stopping criterion, $\|U^{n+1} - U^n\|_2 / \|U^{n+1}\|_2 < 10^{-3}$, where $\|U^{n+1}\|_2$ is the l^2-norm of the vector in (31). All simulations stop at time levels close to each other. In equation (23), we used backward difference in time, but other schemes may be used. In fact, we have used the Crank–Nicolson scheme with LSFEM for transport of pollutants.

4.1. Thermally driven cavity flow

The laminar incompressible flow in a square cavity with insulated top and bottom walls but differentially heated vertical walls has served as the model problem for testing and evaluating numerical techniques for natural convection. We use a non-uniform mesh of 50×50 elements (2601 nodal points, 17 602 degrees of freedom for the thermally driven flow) as shown in Figure 1. The smallest element size is $h = 0{\cdot}002$ at the four corners. The boundary conditions are: $u = v = 0$ everywhere; the top and bottom walls are insulated, $q_y = 0$; the two vertical walls are kept at the uniform temperature, left wall $T = 1$ and right wall $T = 0$; the reference pressure $p = 0$ is specified at the lower left corner. No vorticity ω and heat flux in the x direction q_x are specified. The initial condition is taken as $\mathbf{v}(x, y, 0) = \mathbf{0}$ in the domain Ω. The numerical solutions are obtained for the following dimensionless numbers: $Fr = 1$, $Pr = 0{\cdot}71$ and $Ra = 10^3$, 10^4, 10^5, 10^6. The numerical results are given in Figures 2–4 for contours of temperature and stream function and for velocity vectors. All contour plots compare well with the bench-mark solutions of De Vahl Davis.[25]

The maximum values of velocities u and v and the Nusselt number at the hot wall obtained from the present work are compared with other results reported in the literature,[25–27] as shown in Table I, where Nu_0, Nu_{max} and Nu_{min} are the average Nusselt number, maximum and minimum values of the local Nusselt number at the hot wall ($x = 0$), respectively.

It is worth mentioning that Davis[25] used a streamfunction–vorticity finite difference method with 41×41 grids for $Ra = 10^3$ and $Ra = 10^4$, and 81×81 grids for $Ra = 10^5$ and $Ra = 10^6$. He also used Richardson extrapolation to obtain the bench-mark solutions. Hortmann *et al.*[28] used a finite volume multigrid procedure with 160×160 grids for $Ra = 10^4$ and up to 640×640 grids for $Ra = 10^6$. Ramaswamy *et al.*[27] used a semi-implicit finite element method (a projection scheme including an explicit step for advection terms, fully implicit step for diffusion terms and

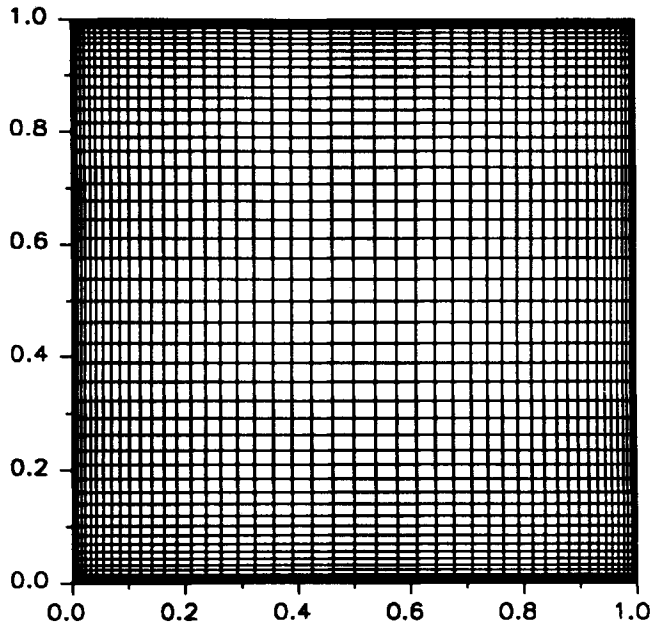

Figure 1. Finite element mesh for thermally driven cavity flow and lid-driven cavity flow (50×50 bilinear elements)

a pressure correction step via the solution of the Poisson equation) with 25×25 biquadratic/bilinear elements for velocity and pressure. In the light of these facts and the results in Table I, our LSFEM results from 50×50 bilinear elements are quite satisfactory.

4.2. Lid-driven cavity flow

The fluid in the cavity is driven by the moving top at an uniform velocity. Since the flow is isothermal, the buoyancy term in equation (10) is neglected, and only equations (9)–(12) are solved. For moderately high Reynolds numbers, Ghia *et al.*[18] used a coupled strongly implicit multigrid method (CSI-GM) to obtain a series of detailed steady-state results with very fine but uniform meshes (129×129 nodal points for $Re \leq 3200$ and 257×257 points for $Re \geq 5000$). Burneau and Jouron[29] also solved this problem for Reynolds numbers as high as 15 000 by means of a multigrid method with a very fine mesh on staggered grids. Finite element solutions by Gresho *et al.*,[19] using a modified finite element method, and by Jiang,[17] using LSFEM, were obtained on grid systems of 50×50 non-uniform bilinear elements for Reynolds numbers up to 10 000. More recently, Ramaswamy *et al.*,[27,30] using a semi-implicit finite element method with biquadratic/bilinear elements on 41×41 and 65×65 non-uniform meshes, presented results for flows up to $Re = 10\,000$.

The boundary conditions are only specified as $u = v = 0$ everywhere except on the top lid, where $u = 1$ and $v = 0$. The reference pressure $p = 0$ is specified at the lower left corner. We do not have to specify vorticity at the cavity wall because Jiang's steady-state results[17] revealed that it was unnecessary to specify vorticity when velocities were specified at the cavity wall. The initial condition is taken as $\mathbf{v}(x, y, 0) = \mathbf{0}$ in the domain Ω.

The numerical results of velocity vector, stream function, pressure contours and vorticity contours for $Re = 5000$, 10 000 are shown in Figures 5 and 6, respectively. The stream function,

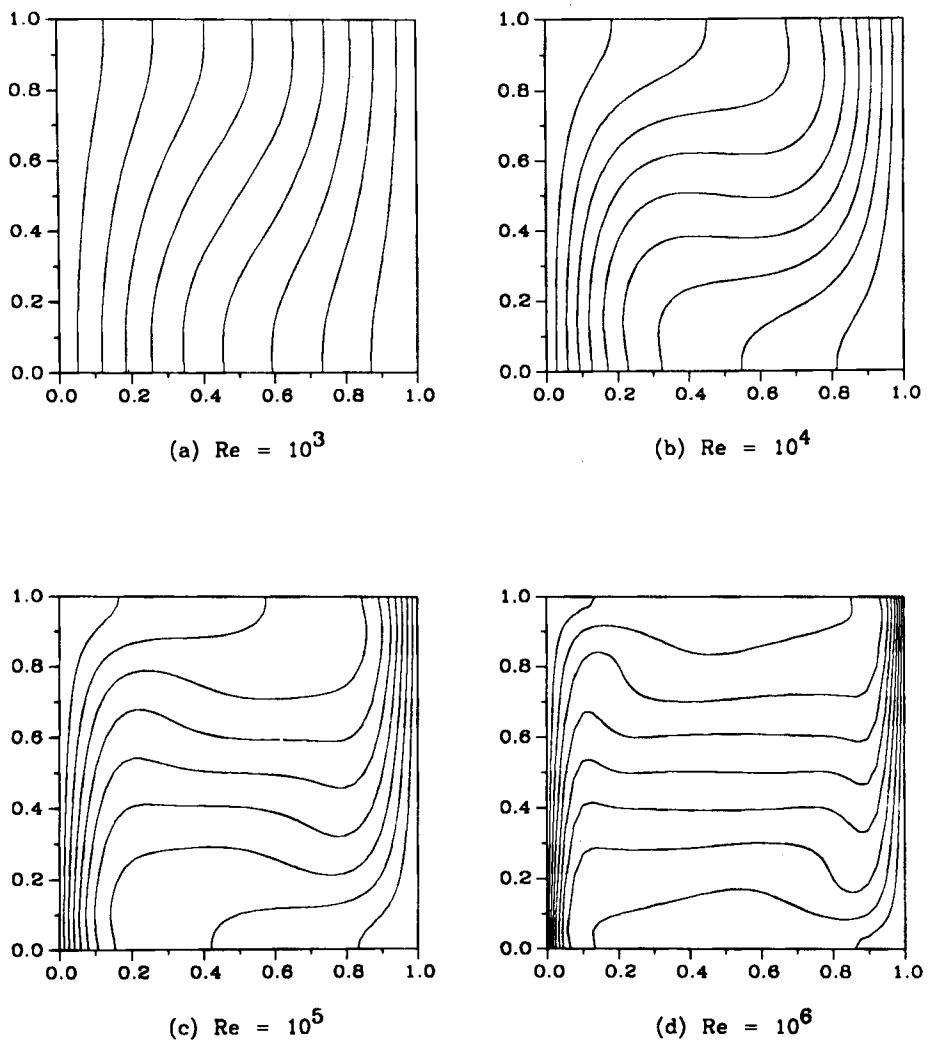

Figure 2. Temperature contours of thermally driven cavity flows at different Rayleigh numbers

vorticity and pressure compare well with those by Ghia *et al.*,[18] Gresho *et al.*[19] and Jiang.[17] As shown in Figure 7, our results for $Re = 10\,000$ at the bottom right corner of the cavity compare well with the fine mesh (257×257) results of Ghia *et al.*[18] Figure 8 shows that the velocity profiles along the central axes of the cavity compare well with those of Ghia *et al.*[18] To achieve 'the steady state', 120 time steps for $Re = 5000$ and 160 time steps for $Re = 10\,000$ are required, with the time step Δt being 0·5.

4.3. Flow over a square obstacle

Whereas the last two examples have often been used to provide bench-mark steady-state solutions to test different numerical algorithms, accurate transient results are scarce in the

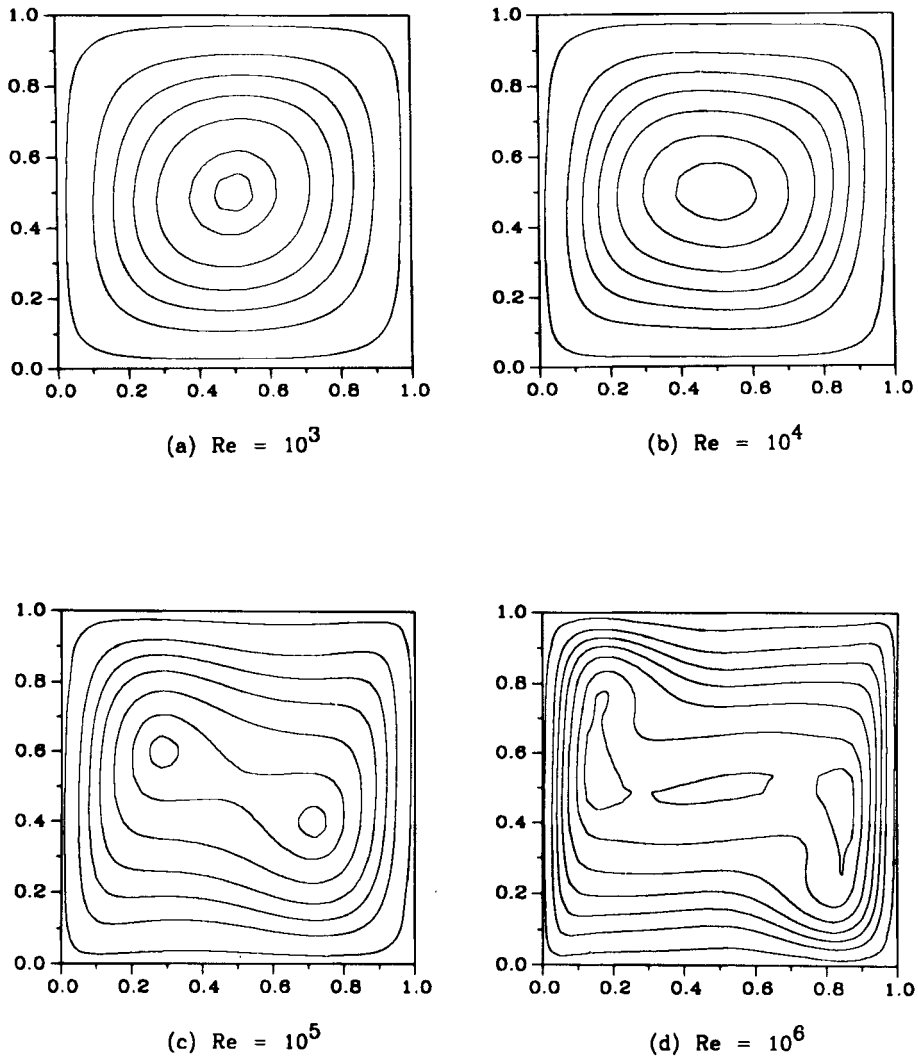

Figure 3. Stream function contours of thermally driven cavity flows at different Rayleigh numbers

literature. For this example, we use LSFEM to simulate the laminar flow over a square obstacle. Using the standard Galerkin finite element method, Leone and Gresho[31] obtained accurate steady-state results, whereas Laval and Quartapelle[32] provided limited transient solutions from a Taylor–Galerkin finite element method.

The geometry of the flow domain and the finite element mesh (totally 950 elements) are given in Figure 9. We consider the problem at $Re=200$. The boundary conditions are set as: at the inlet a constant uniform velocity $u=1$ and $v=0$ are imposed; along the wall and along the obstacle no-slip conditions $u=v=0$ are used. At the outflow boundary, the use of traction-free boundary

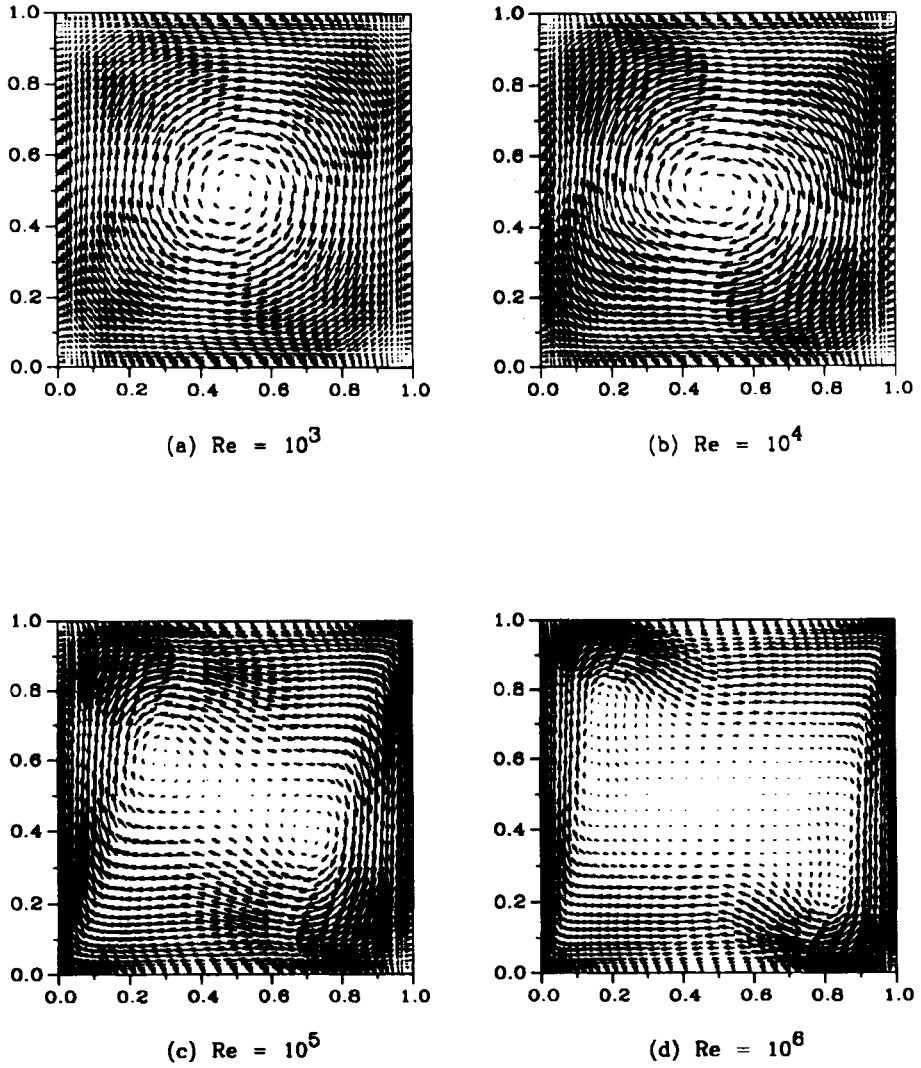

Figure 4. Velocity vectors of thermally driven cavity flows at different Rayleigh numbers

conditions (zero normal and tangential stress) is a common practice (see Reference 31). Since the flow becomes fully developed and unidirectional at the outlet, zero normal stress implies the specification of $p=0$, and zero tangential stress ($\partial u/\partial y=0$) implies that the vorticity is also equal to zero. Therefore, it is reasonable to set vorticity $\omega=0$ and pressure $p=0$ as the outflow boundary condition.

The numerical results for the stream function at $t=1$, 2, 5 and 47 are shown in Figure 10. When $t=47$ (94 time steps), the solution satisfies criterion (37) and is supposed to achieve the steady-state condition. The noteworthy features of the simulation are the presence of velocity vector

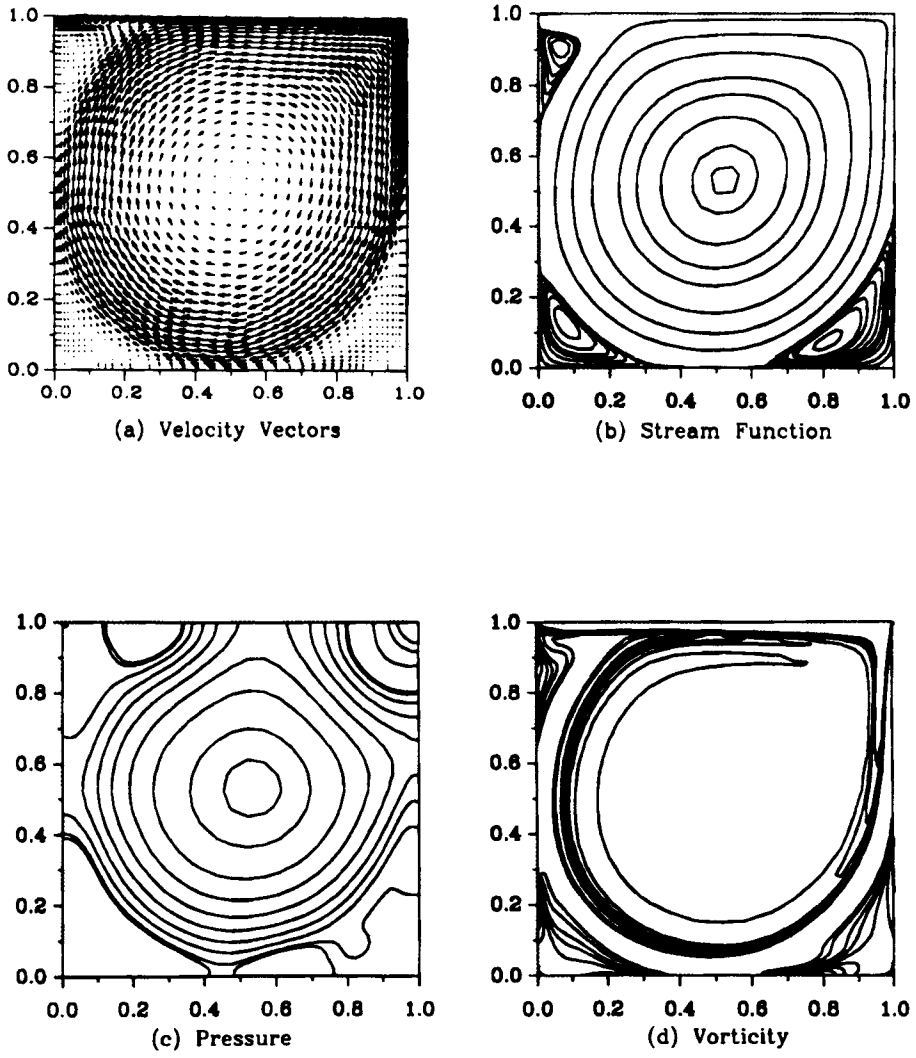

Figure 5. Numerical results of the lid-driven cavity flow for $Re = 5000$ ($t = 60$)

wiggles at the inlet and outlet when a coarse mesh is used. An explanation of the cause of wiggles is given by Leone and Gresho.[31] The vector wiggles can be reduced by using the fine mesh near the corners of the square obstacle as shown in Figure 9. Although LSFEM has 'inherent' numerical diffusion, it does not totally remove wiggles as some upwinding schemes do. Nevertheless, the presence of wiggles signifies the need of local refinement of the mesh system. The velocity vectors at different times are given in Figure 11. The pressure and vorticity contours at $t = 47$ are shown in Figure 12. Our results at $t = 47$ compare well with the steady-state result of Leone and Gresho, whereas our transient results (Figure 10) compare well qualitatively with the results of Laval and Quartapelle.[32]

Table I. Comparison of numerical results

Ra	Source	u_{max}	v_{max}	Nu_0	Nu_{max}	Nu_{min}
	Ramaswamy *et al.*[27]	—	—	—	—	—
	Hortmann *et al.*[28]	—	—	—	—	—
10^3	De Vahl Davis[25]	3·65	3·70	1·12	1·51	0·69
	Present method	3·66	3·68	1·12	1·51	0·69
	Ramaswamy *et al.*[27]	—	19·62	—	—	—
	Hortmann *et al.*[28]	16·18	19·62	—	3·53	—
10^4	De Vahl Davis[25]	16·18	19·62	2·24	3·52	0·59
	Present method	16·24	19·62	2·25	3·53	0·59
	Ramaswamy *et al.*[27]	—	68·62	—	—	—
	Hortmann *et al.*[28]	34·74	68·62	—	7·72	—
10^5	De Vahl Davis[25]	34·73	68·59	4·51	7·72	0·73
	Present method	35·15	68·39	4·52	7·70	0·73
	Ramaswamy *et al.*[27]	—	232·97	—	—	—
	Hortmann *et al.*[28]	64·83	220·47	—	17·54	—
10^6	De Vahl Davis[25]	64·63	219·36	8·82	17·93	0·99
	Present method	65·28	222·09	8·85	17·63	0·95

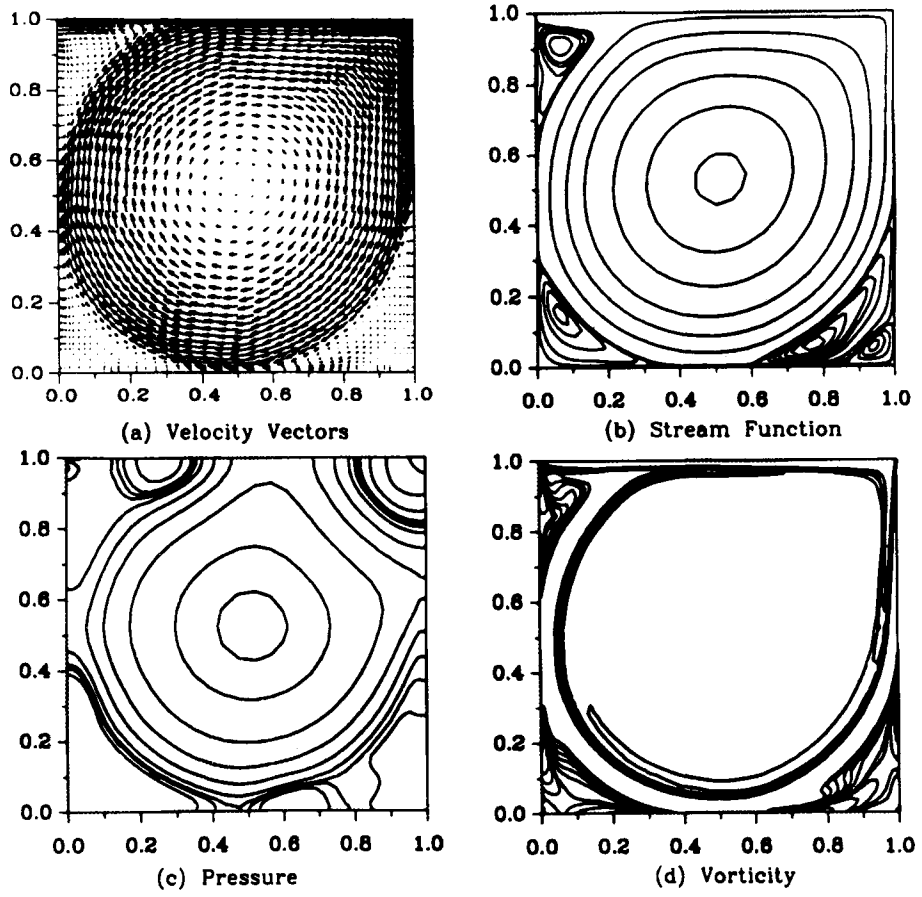

Figure 6. Numerical results of the lid-driven cavity flow for $Re = 10\,000$ ($t = 80$)

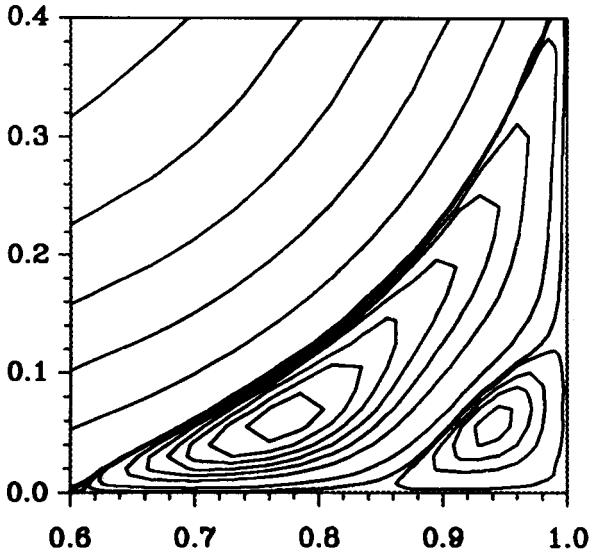

Figure 7. Stream function contours at the lower right corner for $Re = 10\,000$

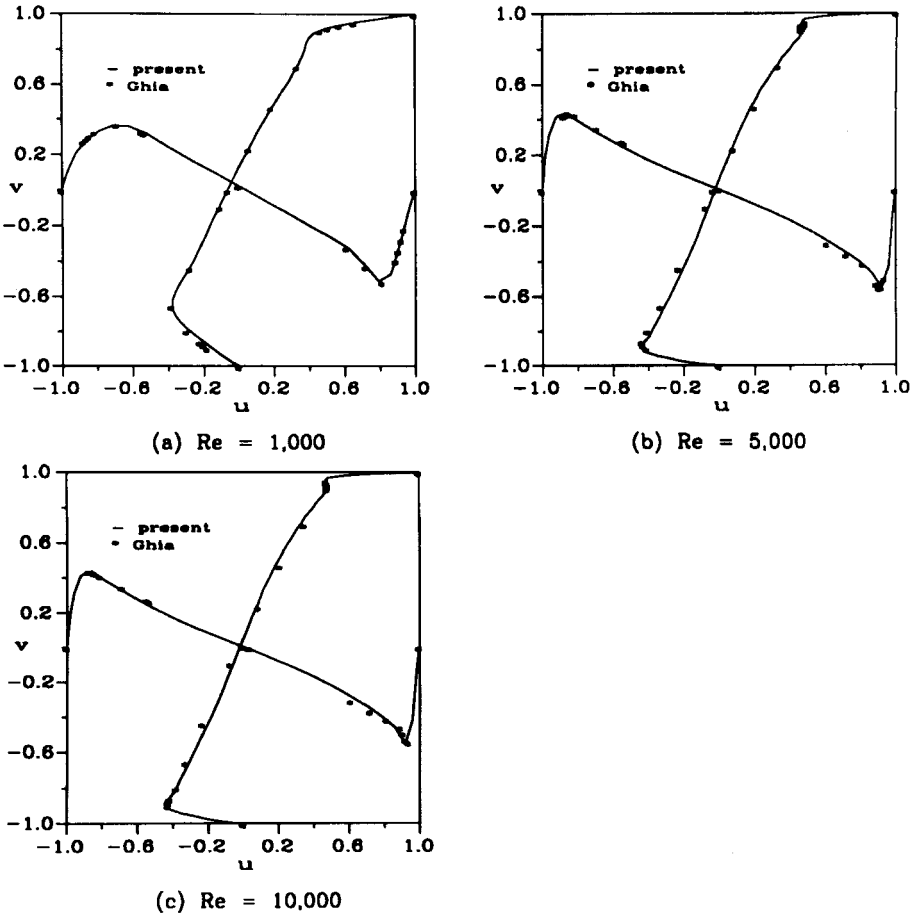

Figure 8. Comparison of velocity profiles through the centre of the cavity

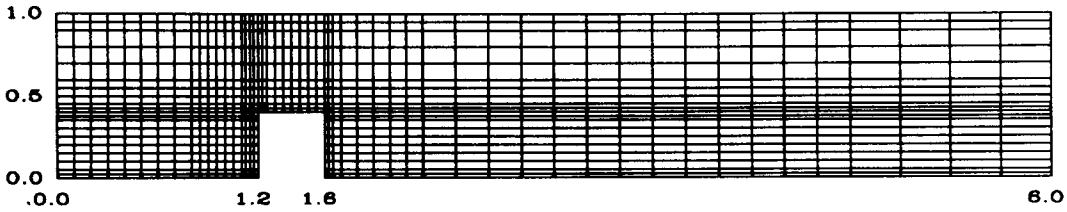

Figure 9. The geometry and finite element mesh for a flow over an obstacle

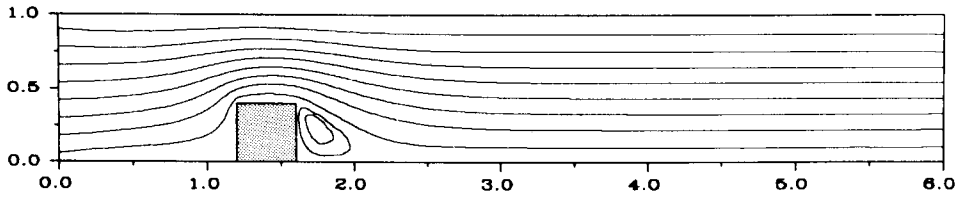

(a) Time = 1.0

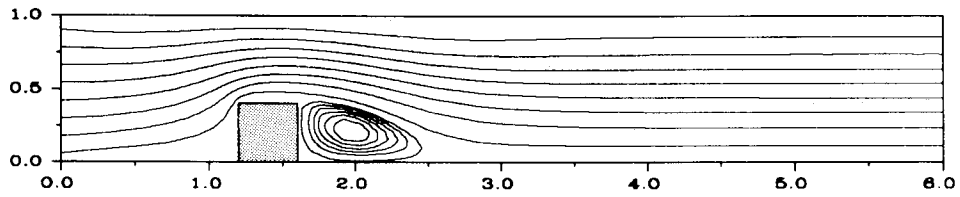

(b) Time = 2.0

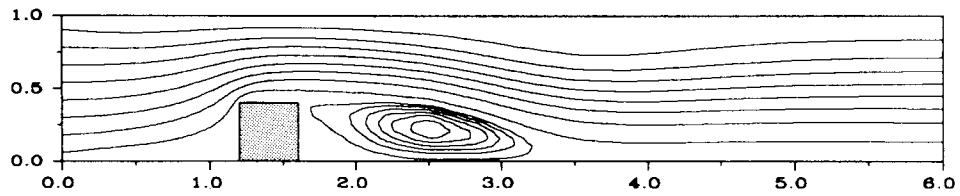

(c) Time = 5.0

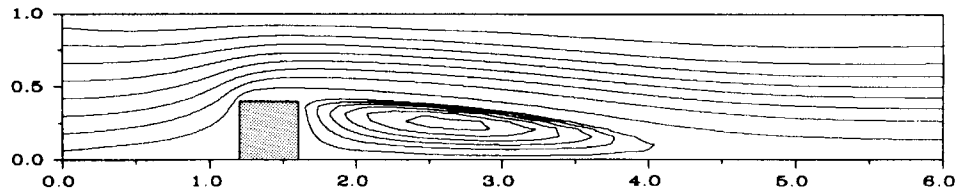

(d) Time = 47

Figure 10. Stream function distribution for flow over an obstacle at $Re=200$

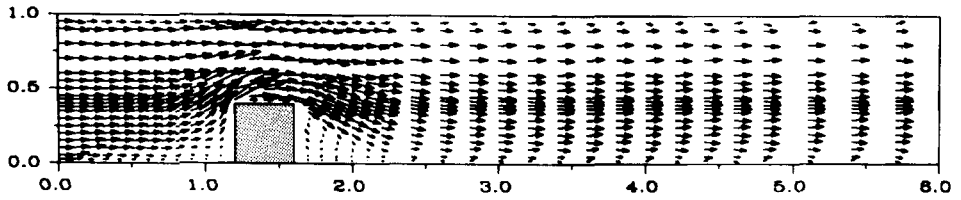

(a) Time = 1.0

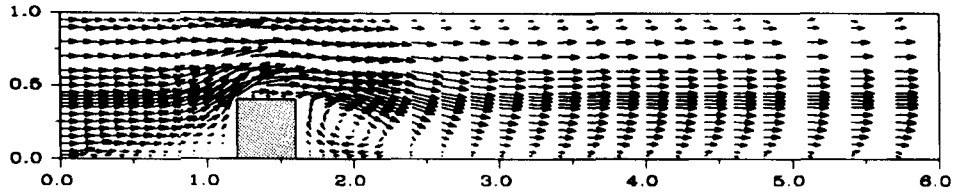

(b) Time = 2.0

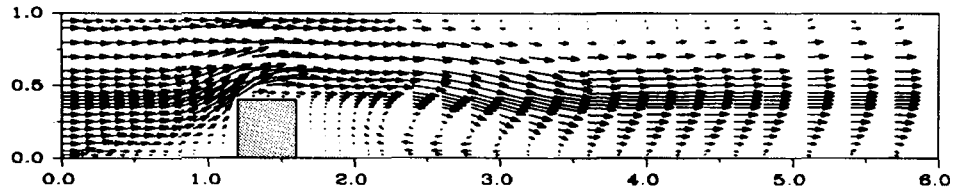

(c) Time = 5.0

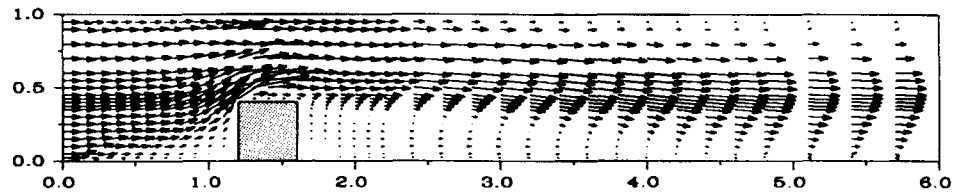

(d) Time = 47

Figure 11. Velocity profile for flow over an obstacle at $Re = 200$

For this problem, the CPU times per time step are 4·5 and 10·4 s, respectively, for using NAG and LINPACK subroutines on a single processor of an IBM 3090-600J computer. The CPU time per time step for the Galerkin finite element method using NAG subroutines is 2·3 s. Since our objective in this work is to test the LSFEM for time-dependent problems, we used the Cholesky decomposition technique to solve the symmetric positive-definite linear systems. In practice, and for large-scale problems, iterative techniques such as preconditioned conjugate gradient methods should be used. For example, Jiang *et al.*[33] have used a matrix-free Jacobi conjugate gradient method for three-dimensional problems.

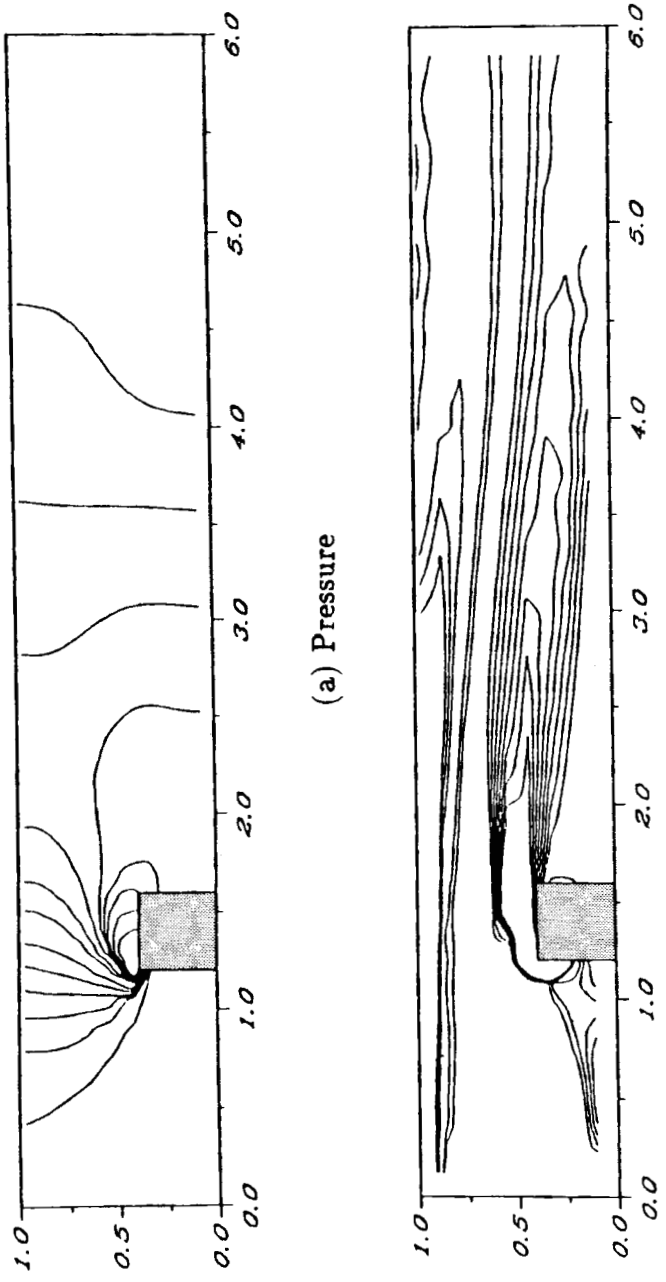

Figure 12. Pressure and vorticity contours at $t=47$ for flow over an obstacle at $Re=200$

5. CONCLUSIONS

A least-squares finite element method has been presented for time-dependent incompressible Navier–Stokes equations and the thermally driven cavity flow problem. The results have demonstrated that the method is reliable, accurate and stable for large time steps. Since the LSFEM provides a Symmetric and Positive-Definite (SPD) matrix system, it has a great deal of potential for time-dependent three-dimensional flow problems. Our preliminary results on the flow over an obstacle also showed that the LSFEM provided accurate numerical solutions for an unbounded physical domain. However, it is obvious that much work remains to be done if LSFEM is to be routinely used for simulating time-dependent three-dimensional flows.

ACKNOWLEDGEMENTS

This work was partially supported by the National Science Foundation (Grant No. ASC-8811171; NSF/KY EPSCoR program). We would like to thank Dr. B. N. Jiang of NASA Lewis Research Center for useful discussions on least-squares finite element methods.

REFERENCES

1. G. F. Carey and J. T. Oden, *Finite Element: Fluid Mechanics*, Vol. VI, Prentice-Hall, Englewood Cliffs, NJ, 1986.
2. J. T. Oden and G. F. Carey, *Finite Element: Mathematical Aspects*, Vol. IV, Prentice-Hall, Englewood Cliffs, NJ, 1983.
3. A. J. Baker, J. W. Kim, J. D. Freels and J. A. Orzechowski, 'On a finite element CFD algorithm for compressible, viscous and turbulent aerodynamics flows', *Int. j. numer. methods fluids*, **7**, 1235–1259 (1987).
4. J. Donea, J. Quartapelle and V. Selmin, 'An analysis of time discretization in the finite element solution of hyperbolic problems', *J. Comput. Phys.*, **70**, 463–499 (1987).
5. T. J. R. Hughes, 'Recent progress in the development and understanding of SUPG methods with special reference to the compressible Euler and Navier–Stokes equations', *Int. j. numer. methods fluids*, **7**, 1261–1275 (1987).
6. B. N. Jiang and G. F. Carey, 'A stable least-squares finite element method for the non-linear hyperbolic problems', *Int. j. numer. methods fluids*, **8**, 933–942 (1988).
7. B. N. Jiang and G. F. Carey, 'Least-squares finite elements for compressible Euler equations', *Int. j. numer. methods fluids*, **10**, 557–568 (1990).
8. B. N. Jiang and L. A. Povinelli, 'Least-squares finite element method for fluid dynamics', *Comput. methods appl. mech. eng.*, **8**, 13–37 (1990).
9. D. Lefebvre, J. Peraire and K. Morgan, 'Least squares finite element solution of compressible and incompressible flows', *Int. J. Numer. Methods Heat Transfer Fluid Flow* (to be published).
10. J. Donea and J. Quartapelle, 'An introduction to finite element methods for transient advection problems', *Comput. Methods appl. mech. eng.*, **95**, 169–203 (1992).
11. C. W. Li, 'Least square-characteristics and finite elements for advection–dispersion simulation', *Int. j. numer. methods eng.*, **29**, 1343–1364 (1990).
12. G. F. Carey and B. N. Jiang, 'Least-squares finite elements for first-order hyperbolic systems', *Int. j. numer. methods eng.*, **26**, 81–93 (1988).
13. N. S. Park and J. A. Liggett, 'Taylor-least squares finite element for two-dimensional advection dominated advection–diffusion problems', *Int. j. numer. methods fluids*, **11**, 21–28 (1990).
14. H. Nguyen and J. Reynen, 'A space–time least-squares finite element scheme for advection–diffusion equations', *Comput. methods appl. mech. eng.*, **42**, 331–342 (1984).
15. C. L. Chang and B. N. Jiang, 'An error analysis of least-squares finite element method of velocity–pressure–vorticity formulation for Stokes problem', *Comput. methods appl. mech. eng.*, **84**, 247–255 (1990).
16. B. N. Jiang and C. L. Chang, 'Least-squares finite elements for the Stokes problem', *Comput. methods appl. mech. eng.*, **78**, 297–311 (1990).
17. B. N. Jiang, 'A least-squares finite element method for incompressible Navier–Stokes problems', *Int. j. numer. methods fluids*, **14**, 843–859 (1992).
18. U. Ghia, K. N. Ghia and C. T. Shin, 'High-*Re* solutions for incompressible flow using the Navier–Stokes equations and multigrid method', *J. Comput. Phys.*, **48**, 387–411 (1982).
19. P. M. Gresho, S. T. Chan, R. L. Lee and C. D. Upson, 'A modified finite element method for solving the time-dependent, incompressible Navier–Stokes equations. Part 2: applications, *Int. j. numer. methods fluids*, **4**, 619–640 (1984).
20. S. W. Kim, 'A fine grid finite element computation of two-dimensional high Reynolds number flows', *Comput. Fluids*, **16**, 429–444 (1988).

21. J. L. Sohn, Y. Kim and T. J. Chung, 'Finite element solver for incompressible fluid flow and heat transfer', in T. J. Chung and G. R. Karr (eds), *Finite Element Analysis in Fluid, Proc. 7th Int. Conf. on Finite Element Methods in Flow Problems*, UAH Press, Huntsville, AL, 1989, pp. 880–885.
22. P. M. Gresho, 'Incompressible fluid dynamics: some fundamental formulation issue', *Annu. Rev. Fluid Mech.*, **23,** 413–453 (1991).
23. O. C. Zienkiewicz, D. R. J. Owen and K. N. Lee, 'Least squares finite element for elastostatic problems—use of reduced integration', *Int. j. numer. methods eng.*, **8,** 341–358 (1974).
24. R. Sani, P. Gresho, R. Lee and D. Griffiths, 'The cause and cure (?) of the spurious pressure generated by certain FEM solutions of the incompressible Navier–Stokes equations: Part 1 and Part 2', *Int. j. numer. methods fluids*, **1,** 17–43, 171–204 (1981).
25. G. De Vahl Davis, 'Natural convection of air in a square cavity: a bench mark numerical solution', *Int. j. numer. methods fluids*, **3,** 249–264 (1983).
26. G. De Vahl Davis and I. P. Jones, 'Natural convection in a square cavity: a comparison exercise', *Int. j. numer. methods fluids*, **3,** 227–248 (1983).
27. B. Ramaswamy, T. C. Jue and J. E. Akin, 'Finite-element analysis of unsteady two-dimensional Navier–Stokes equations', *Numer. Heat Transfer*, Part B, **21,** 147–182 (1992).
28. M. Hortmann, M. Peric and G. Scheuerer, 'Finite element multigrid prediction of laminar natural convection: bench-mark solutions', *Int. j. numer. methods fluids*, **11,** 189–207 (1990).
29. C. H. Bruneau and C. Jouron, 'An efficient scheme for solving steady incompressible Navier–Stokes equations', *J. Comput. Phys.*, **89,** 389–413 (1990).
30. B. Ramaswamy, T. C. Jue and J. E. Akin, 'Semi-implicit and explicit finite element schemes for coupled fluid/thermal problems', *Int. j. numer. methods eng.*, **34,** 675–696 (1992).
31. J. M. Leone Jr. and P. M. Gresho, 'Finite element simulations of steady, two-dimensional, viscous incompressible flow over a step', *J. Comput. Phys.*, **41,** 167–191 (1981).
32. H. Laval and L. Quartapelle, 'A fractional-step Taylor–Galerkin method for unsteady incompressible flows', *Int. j. numer. methods fluids*, **11,** 501–513 (1990).
33. B. N. Jiang, T. L. Lin and L. A. Povinelli, 'Large-scale computation of incompressible viscous flow by least-squares finite element method', *Comput. methods appl. mech. eng.* (submitted).
34. M. O. Bristeau, O. Pironneau, R. Glowinski, J. Periaux and P. Perrier, 'On the numerical solution of nonlinear problems of fluid dynamics by least square and finite element methods—Part I. Least squares formulations and conjugate gradient solutions of the continuous problems', *Comput. methods appl. mech. eng.*, **17/18,** 619–657 (1979).